Journal of Hydrology 640 (2024) 131660

Contents lists available at ScienceDirect

Journal of Hydrology

journal homepage: www.elsevier.com/locate/jhydrol

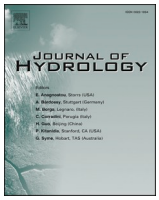

Research papers

Efficient modelling of lateral discharge through a dike breach

Vincent Schmitz [a,*], Vasileios Kitsikoudis [b], Gregoire Wylock [a], Sebastien Erpicum [a], Michel Pirotton [a], Pierre Archambeau [a], Benjamin Dewals [a]

[a] Hydraulics in Environmental and Civil Engineering, Urban and Environmental Engineering, University of Liege, 4000 Liege, Belgium
[b] Water Engineering and Management, Faculty of Engineering Technology, University of Twente, 7500 AE Enschede, The Netherlands

ARTICLE INFO

This manuscript was handled by Corrado Corradini, Editor-in-Chief, with the assistance of Zhang Wen, Associate Editor

ABSTRACT

Breaches in fluvial dikes can lead to major flooding in the hinterland with severe societal and economic consequences. The discharge partitioning at the location of a dike breach is a complex flow phenomenon with 2D and 3D flow features that needs to be predicted accurately for the estimation of flood hazard. Determining the exact location of a potential breach is highly uncertain and so are the circumstances in which it could appear. Therefore, many scenarios should be investigated. Fast and accurate modelling of the discharge partitioning with appropriate simplifications and parameterizations are required to allow for a large number of simulations within reasonable computational time. To achieve this, spatially lumped or one-dimensional flow models have been used in combination with side weir equations. For the first time, the present study systematically assesses the performance of eleven side weir equations for the determination of the lateral discharge through a breach in a dike that is parallel to the flow direction along a straight river reach. These side weir equations were implemented in a zero-dimensional spatially lumped flow model and in a one-dimensional spatially distributed flow model. Both models were evaluated against experimental data from laboratory tests with a side opening that was either fixed, or dynamically evolving. The performance of the side weir equations varied with the experimental data, highlighting the empirical nature of most of these equations. The coupling of the side weir equations with the spatially distributed flow model did not always generate better results than the coupling with the lumped model, which implies that increasing the model complexity does not systematically lead to better predictions of the dike breach discharge.

1. Introduction

Fluvial dikes or levees are engineered structures that confine the river flow at high discharges and provide flood protection. Several mechanisms can lead to a dike failure, such as overtopping (Rifai et al., 2017), slumping failure (Elalfy et al., 2018), piping (Vorogushyn et al., 2009), seepage (Onda et al., 2019), and the weakening of some parts of the dike caused by the actions of burrowing animals and poor maintenance (Orlandini et al., 2015). The failure of a fluvial dike can induce major flooding in the hinterland with detrimental consequences to local economies and potentially life losses, especially in urbanized areas. Thus, the accurate prediction of the dike breach hydrograph is of paramount importance for the estimation of flood hazard and for the determination of safe evacuation routes, especially when considering the fact that people tend to settle within flood sheltered areas (Haer et al., 2020). This kind of river flood risk is expected to increase in the future, as more people are exposed to floods (Tellman et al., 2021) and extreme precipitation is projected to increase (Madsen et al., 2014).

The discharge partitioning in a channel with a side opening is inherently a 2D and 3D flow phenomenon (Stilmant et al., 2013; Li et al., 2021; Dewals et al., 2023) with flow separation, flow recirculation, and helicoidal flow near the side opening (Michelazzo et al., 2015). The lateral flow discharge through a side opening has been modelled successfully using 2D models (Roger et al., 2009; Yu et al., 2013; Echeverribar et al., 2019; Shustikova et al., 2020). Recent studies have coupled 2D hydraulic models with physically-based erosion models (Kakinuma and Shimizu, 2014; Elalfy et al., 2018; Dazzi et al., 2019). Also, 1D-2D hydraulic models were extended using additional computational elements, such as a physically-based description of the breach formation and evolution (Viero et al., 2013). Another example is the use of probabilistic frameworks for possible locations and timing of breaches along a dike with the aid of fragility curves for various failure

* Corresponding author.
E-mail address: v.schmitz@uliege.be (V. Schmitz).

https://doi.org/10.1016/j.jhydrol.2024.131660
Received 15 April 2024; Received in revised form 19 June 2024; Accepted 28 June 2024
Available online 16 July 2024
0022-1694/© 2024 Elsevier B.V. All rights are reserved, including those for text and data mining, AI training, and similar technologies.

mechanisms (Vorogushyn et al., 2010; Bomers et al., 2019; D'Oria et al., 2019; Maranzoni et al., 2022). Despite recent advancements (Dazzi et al., 2019; Ferrari et al., 2020), such models have either long computational times or large uncertainties regarding their parameterizations. This can become prohibitive for systematic analyses of the flood hazard from dike breaches since breaches at different dike locations can lead to different flood patterns. There is a need for simpler and faster modelling procedures that approximate the complex hydrodynamic processes near and through a dike breach. This is particularly relevant for sensitivity analysis (Schmitz et al., 2023a) and for inclusion in river models, which are also subject to further simplifications (Kitsikoudis et al., 2020), for systematic flood risk assessment.

Side weir equations provide an easy parameterization of the lateral discharge through a side opening. While side weir equations have been applied to fluvial dike breaches (Kamrath et al., 2006; Yu et al., 2013; Wei et al., 2016), the number of such studies is small compared to those modelling frontal dike breaches or earthen embankment breach as a frontal weir (ASCE/EWRI Task Committee, 2011; Schmocker and Hager, 2012; Wu, 2013). As a result, the accuracy of the side weir equations and the parameterization of the side weir discharge coefficient, C_d, for breaches in fluvial dikes have not been thoroughly evaluated yet. Mignot et al. (2020) assessed the predictive capability of eleven semi-empirical formulations for C_d. To this end, they used laboratory experiments of flow intrusion into buildings and considered the building openings (doors, windows, and gates) as rectangular side weirs. The computed side discharge was highly dependent on the formulation of C_d. The applicability of such semi-empirical equations to fluvial dike breaches is not straightforward. Dike breaches exhibit a time-dependent complex geometry, i.e., a dynamically evolving and uneven breach profile (Rifai et al., 2017), that depends on the discharge in the main channel, and the dike geometry and erodibility (Schmitz et al., 2021).

Rifai et al. (2017, 2018) identified three stages during the development of a non-cohesive dike breach caused by overtopping (Fig. 1). Initially, right after overtopping occurs, the erosion rate of the dike is low because the flow depth and the velocity above the dike are also small. As the flow depth and the velocity above the dike breach increase, erosion intensifies rapidly with large water level variations near the breach (Al-Hafidh et al., 2022) and a downstream shift of the breach center. Finally, in the last stage, the upstream side of the breach remains almost fixed, and the breach grows more slowly in the downstream direction.

Similar observations were reported by Michelazzo et al. (2018) and Kakinuma and Shimizu (2014) from laboratory-scale and field-scale experiments, respectively. Overall, the dike breaching process is accelerated and the final shape of the breach gets larger with increasing water level and flow discharge in the river (Yu et al., 2013; Rifai et al., 2017; Wu et al., 2018). The dike composition also affects the breach expansion (Yu et al., 2013; Wu et al., 2018; Rifai et al., 2021), so does the channel width (Schmitz et al., 2023b) and the dike geometry, with dikes with larger volume per unit width inducing a more gradual enlargement of the breach during the rapid expansion phase (Schmitz et al., 2021). The breach location and its final shape govern to a large extent the flood inundation (Tadesse and Fröhle, 2020). The water level in the hinterland (Rifai et al., 2018) and the presence or not of riprap also alter the breach development (Ahadiyan et al., 2022).

The present study investigates the suitability of different parameterizations for lateral flow through dike breaches for the incorporation of 3D flow processes into simpler and faster models. Specifically, this study assesses the performance of eleven semi-empirical side weir equations applied in two different modelling frameworks to determine the lateral outflow discharge through a breach in a dike that is parallel to the flow main direction along a straight river reach. The assessment is performed in two frameworks: by combining the side weir equations with either a spatially lumped flow model based on mass conservation or a one-dimensional flow model based on the shallow water equations. The semi-empirical side weir equations, coupled with the two models, are firstly tested with data from channels with fixed side openings and secondly with data from a channel with a dynamic evolution of a dike breach.

Section 2 presents the numerical models used in this work. Section 3

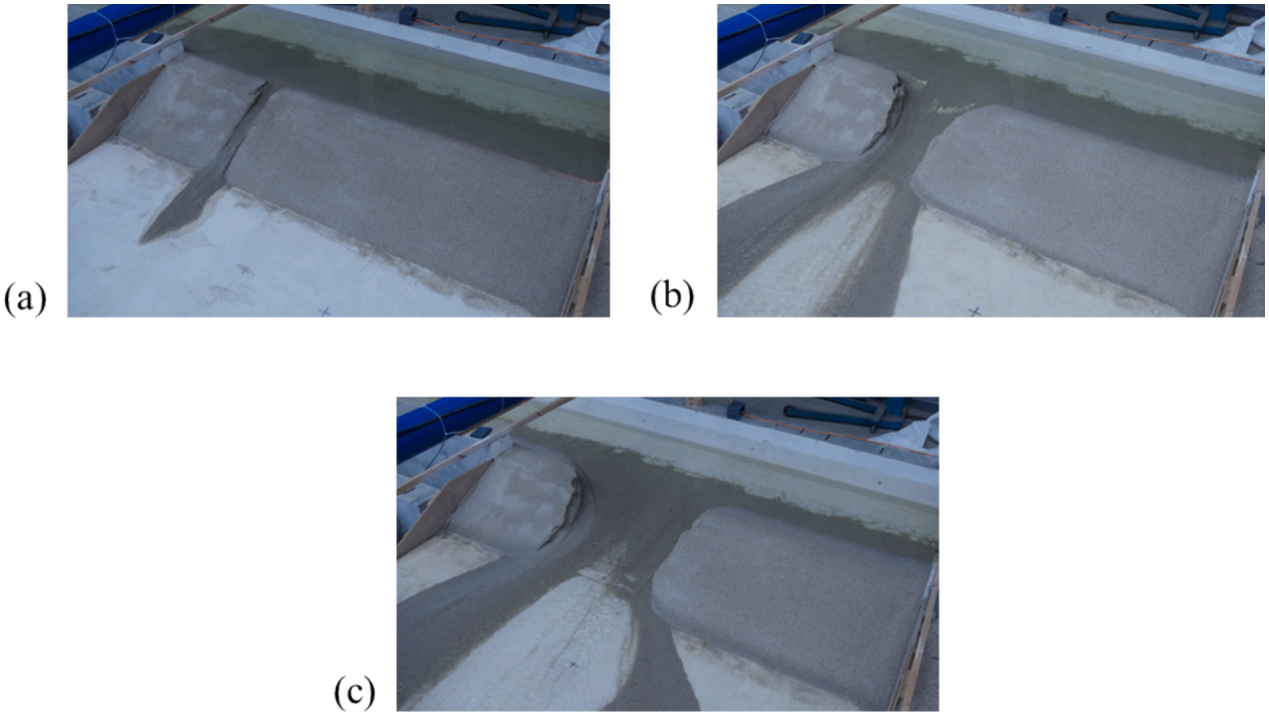

Fig. 1. Three stages observed during a non-cohesive homogeneous dike breaching event due to overtopping: (a) initial low erosion phase, (b) erosion intensification period, and (c) erosion stabilization phase. The corresponding experimental test was performed at the "Laboratoire d'hydraulique des constructions" of the University of Liège, Belgium.

briefly presents the experimental data from the literature that are used for the validation of the developed models (three experiments with a lateral outflow through a fixed geometry and one experiment with an evolving dike breach geometry). Section 4 presents how the breach discharge predicted by the semi-empirical equations compares with the experimental measurements. The performance and limitations of the models are discussed in Section 5. Finally, conclusions are drawn in Section 6.

2. Modelling of the lateral flow discharge through a dike breach

2.1. Discharge coefficient for lateral side weirs

The lateral flow discharge through a breach in a dike that runs parallel to the flow direction in a straight river reach with width W (Fig. 2) can be simplified as a flow over a broad-crested rectangular side weir. In such a case, the incoming flow discharge from the upstream of the channel, Q_{in}, is divided at the location of the dike breach into the lateral flow discharge, Q_b, towards the hinterland and the outgoing flow discharge, Q_{out}, towards the downstream of the channel. In a straight channel, the lateral flow discharge over a rectangular side weir is expressed as:

$$Q_b = \frac{2}{3} C_d \sqrt{2g(h-p)^3} L_s \tag{1}$$

where C_d is the side weir discharge coefficient, h is the flow depth in the main channel upstream of the side opening, p is the crest height of the side weir, L_s is the length of the side weir, and g is the acceleration of gravity. The discharge coefficient, C_d, is typically estimated from analytical and semi-empirical relationships based on the weir and flow characteristics. Similarly to Mignot et al. (2020), eleven relationships from the literature for the calculation of C_d for sharp-crested weirs are used in this study (Table 1).

2.2. Numerical models for flow through a dike breach

Two simplified models were developed using *MATLAB* software to predict the lateral flow discharge, Q_b, through a side opening representing a dike breach. Section 2.2.1 presents a lumped model and Section 2.2.2 presents a one-dimensional finite volume model. Both models are coupled with Eq. (1) and with an equation for the determination of C_d (Table 1).

2.2.1. Lumped model (zero-dimensional)

The lumped model is based on a side weir discharge equation for the determination of Q_b(Eq. (1)) and on the mass balance equation in a control volume, which writes:

$$\frac{dV}{dt} = A_{xy}(h_{xy}) \frac{dh_{xy}}{dt} = Q_{in} - Q_b(h_{xy}) - Q_{out}(h_{xy}) \tag{2}$$

where V is the volume of water in the control volume, t is the time, A_{xy} is the horizontal surface area of the control volume, and h_{xy} is the flow depth spatially averaged across the area A_{xy}.

This numerical model estimates the spatially averaged flow depth h_{xy} for every timestep dt, based on the value of h_{xy} in the previous timestep, the measured value of Q_{in}, an experimental rating curve for Q_{out}, and the value of Q_b computed at the previous timestep with Eq. (1). The surface area A_{xy} is considered as constant in each case.

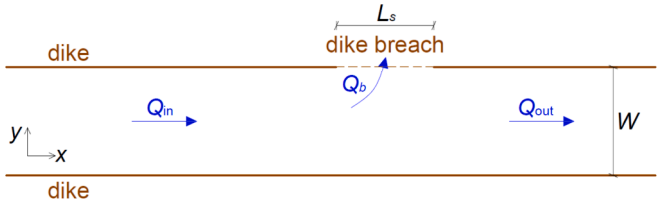

Fig. 2. Flow within a straight channel with a dike breach on the side.

2.2.2. Spatially distributed model (one-dimensional)

The spatially distributed model solves numerically the one-dimensional Saint-Venant equations, i.e., the conservation of mass (Eq. (3)) and the conservation of momentum (Eq. (4)):

$$\frac{\partial A}{\partial t} + \frac{\partial Q}{\partial x} = -q_b \tag{3}$$

$$\frac{\partial Q}{\partial t} + \frac{\partial}{\partial x}(QU + gAy) + gA(S_f - S_0) = -Uq_b \tag{4}$$

where A is the flow cross-sectional area, Q is the discharge in the channel, q_b is the specific lateral discharge through the side opening, U is the longitudinal velocity averaged over the cross-section, y is the cross-section average of the depth, S_f is the friction slope, and S_0 is the bed slope. By considering $U = Q/A$, expressing y as a function of the cross-sectional area, $y = f(A)$, and estimating the friction slope with the Manning formula, the only remaining unknowns in Eqs. (3) and (4) are Q and A.

Eqs. (3) and (4) are discretized spatially with a finite volume numerical scheme (Kerger et al., 2011) and in time with a two-step Runge-Kutta algorithm. q_b is computed on each spatial step, Δx, as a function of the local water depth and the local height of the side weir crest (h and p are considered constant over each cell). Δx was 1 cm in the experiments of Michelazzo et al. (2015) and Mignot et al. (2020), and 10 cm in the experiments of Roger et al. (2009) and Rifai et al. (2017) (see Section 3).

2.3. Initial and boundary conditions

The initial water level in the main channel for each simulation was the same as the water level under steady flow conditions with the prescribed incoming discharge, Q_{in}, of the corresponding experiment but without a dike breach. In practice, this water level was computed using our numerical models without considering any breach discharge. The equilibrium breach discharge was obtained when the flow reached a new steady state in the presence of a dike breach. The downstream boundary condition was a rating curve at the weir (Roger et al., 2009), sluice gate (Michelazzo et al., 2015), crested tailgate (Mignot et al., 2020), or perforated plate (Rifai et al., 2017) of each experiment.

3. Experimental data

The accuracy of the eleven semi-empirical side discharge equations (Section 2.1) is evaluated by comparing the modelling results with experimental data from the literature. The considered experimental data comprise data from (a) experiments with a fixed side opening (Roger et al., 2009; Michelazzo et al., 2015; Mignot et al., 2020) and (b) experiments with a dynamically evolving side opening (Rifai et al., 2017). In all experiments, the side opening was parallel to the main flow direction and in a straight channel (Fig. 2), which had uniform and steady flow characteristics. The experimental setups and methods used to generate these data are briefly described in this section and summarized in Table 2. The setup used for each test campaign is displayed in Fig. 3. More details can be found in the referenced studies.

3.1. Experiments with fixed geometry of the side opening

3.1.1. Experiments of Roger et al. (2009)

Roger et al. (2009) carried out laboratory experiments of a dike breach in a 1 m-wide rectangular flume. The rectangular side opening was 0.7 m long and its crest had zero height, simulating the complete failure of a dike. The lateral discharge through the side opening was propagated into a 3.5 × 4.0 m^2 basin that was at the same level as the

Table 1
Formulas for the estimation of the side weir discharge coefficient, C_d, and the associated ranges of $Fr(=U/\sqrt{gh})$, p/h, and L_s/W for which these formulas were developed. Fr and h were measured at the channel centerline, just upstream from the side breach. The table is adapted from Mignot et al. (2020).

No	Source	$C_d(-)$	Fr(−)	$p/h(-)$	$L_s/W(-)$
1	Nadesamoorthy and Thomson (1972)	$0.432\left(\frac{2+\mathrm{Fr}^2}{1+2\mathrm{Fr}^2}\right)^{0.5}$	0.02 – 4.3	0 – 0.96	0.2 – 1
2	Subramanya and Awasthy (1972)	$0.611\left(1-\frac{3\mathrm{Fr}^2}{2+\mathrm{Fr}^2}\right)^{0.5}$	0.02 – 0.9	0.2 – 0.96	0.2 – 1
3	Yu-Tek (1972)	$0.622-0.222\mathrm{Fr}$	0.02 – 4.3	0 – 0.96	0.2 – 1
4	Ranga Raju et al. (1979)	$0.81-0.6\mathrm{Fr}$	0.1 – 0.5	n/a	0.33 – 0.5
5	Hager (1987)	$0.636\left(1+\frac{(H-p)^3}{7H^3}\right)\left(\frac{H-p}{3H-2h-p}\right)^{0.5}$	Analytical approach		
6	Singh et al. (1994)	$0.33-0.18\mathrm{Fr}+0.49\frac{p}{h}$	0.22 – 0.42	0.45 – 0.85	0.4 – 0.8
7	Swamee et al. (1994)	$0.447\left[\left(\frac{44.7p}{49p+h}\right)^{6.67}+\left(\frac{h-p}{h}\right)^{6.67}\right]^{-0.15}$	0.1 – 0.93	0 – 0.31	0.4 – 1
8	Jalili and Borghei (1996)	$0.71-0.41\mathrm{Fr}-0.22\frac{p}{h}$	0.1 – 2	0.05 – 0.87	0.67 – 2.5
9	Borghei et al. (1999)	$0.7-0.48\mathrm{Fr}-0.3\frac{p}{h}+0.06\frac{L_s}{W}$	0.1 – 0.9	0.02 – 0.87	0.33 – 2.33
10	Emiroglu et al. (2011)	$\left[0.836+\left(-0.035+0.39\left(\frac{p}{h}\right)^{12.69}+0.158\left(\frac{L_s}{W}\right)^{0.59}+0.049\left(\frac{L_s}{h}\right)^{0.42}+0.244\mathrm{Fr}^{2.125}\right)^{3.018}\right]^{5.36}$	0.08 – 0.92	0.34 – 0.91	0.3 – 3
11	Bagheri et al. (2014)	$-1.423\mathrm{Fr}^{0.138}+0.744\left(\frac{h-p}{L_s}\right)^{-0.083}+0.723\left(\frac{h-p}{p}\right)^{0.088}+0.182\left(\frac{L_s}{W}\right)^{-0.241}$	0.08 – 0.91	0.22 – 0.9	0.5 – 1.5

Table 2
Main characteristics of the experimental tests considered in this study.

	Fixed breach geometry				Dynamic breach geometry
	Zero lateral crest height			Non-zero lateral crest height	
Source	Roger et al. (2009)	Michelazzo et al. (2015)	Mignot et al. (2020)	Mignot et al. (2020)	Rifai et al. (2017)
Number of tests	4	10	4	2	4
Channel width (m)	1	0.3	0.79	0.79	1
Channel length (m)	9	5.1	8.35	8.35	10
Slope (%)	–	0.3	0.18	0.18	–
Breach length (m)	0.7	0.03 – 0.47	0.079	0.154	dynamic
Manning coefficient ($s/m^{1/3}$)	0.015	0.024	0.01	0.01	0.018
$Q_{in}(m^3/s)$	0.2 and 0.3	~0.01	$5.78{\cdot}10^{-4}$ – $4.19{\cdot}10^{-3}$	$1.142{\cdot}10^{-3}$ and $1.273{\cdot}10^{-3}$	0.02 – 0.05
Downstream boundary condition	weir	sluice gate	crested tailgate	crested tailgate	perforated plate

flume bottom and was made of glass. The water flowed freely off the edges of the basin, while at the downstream end of the flume the water flowed over a weir. The tested inflow discharges were equal to 0.2 m^3/s and 0.3 m^3/s and the tested undisturbed flow depths were 0.4 and 0.5 m, resulting in four experimental combinations in total.

3.1.2. *Experiments of Michelazzo et al. (2015)*

Michelazzo et al. (2015) conducted laboratory experiments in a 30 cm wide recirculating flume with a slope of 0.1 % and rectangular cross section. Fine gravel was glued on the bed of the flume to provide roughness. A vertical sluice gate was placed at the downstream extremity of the flume to adjust the flow depth. A rectangular side weir with zero height diverted a portion of the flow to a lateral channel at a lower level, which conveyed water toward a storage basin through its downstream end. Ten different side weir lengths were tested and varied from 3 to 47 cm. In all cases, the incoming discharge was about 0.01 m^3/s while the sluice gate at the downstream end of the flume was always set in the same way.

3.1.3. *Experiments of Mignot et al. (2020)*

Mignot et al. (2020) investigated the flow intrusion from a flooded street into buildings through openings, such as doors, gates, and windows, during urban floods. The flow through building openings, without nearby obstacles, can be considered as flow through a rectangular side weir with zero and non-zero crest height for doors/gates and windows, respectively. Alternatively, these cases can represent the total or partial collapse of a dike section. The experiments were carried out in a 0.79 m-wide flume with a smooth bed and a rectangular cross section. The slope of the flume was 0.18 % and the flow depth was regulated by a sharp crested tailgate at the downstream end of the flume. The side opening was 7.9 cm long for the cases with zero weir crest height and 15.4 cm long for the cases with non-zero weir crest height. Four and two inflow discharges were tested with zero and non-zero weir crest height, respectively. Mignot et al. (2020) also investigated the impact of urban obstacles, such as parked cars, on the flow intrusion but these cases are not considered in this study.

3.2. *Experiments of Rifai et al. (2017) with dynamic evolution of the geometry of the side opening*

Rifai et al. (2017) investigated the evolution of a breach in a sandy homogeneous trapezoidal dike due to overtopping. The experiments were conducted in a 10 m-long and 1 m-wide flume with a trapezoidal cross section. The erodible dike stretched over 3 m along the right side of the flume and separated the flume from a 4.3 m x 2.5 m area behind the dike. The bottom of this area and of the main flume was coated with

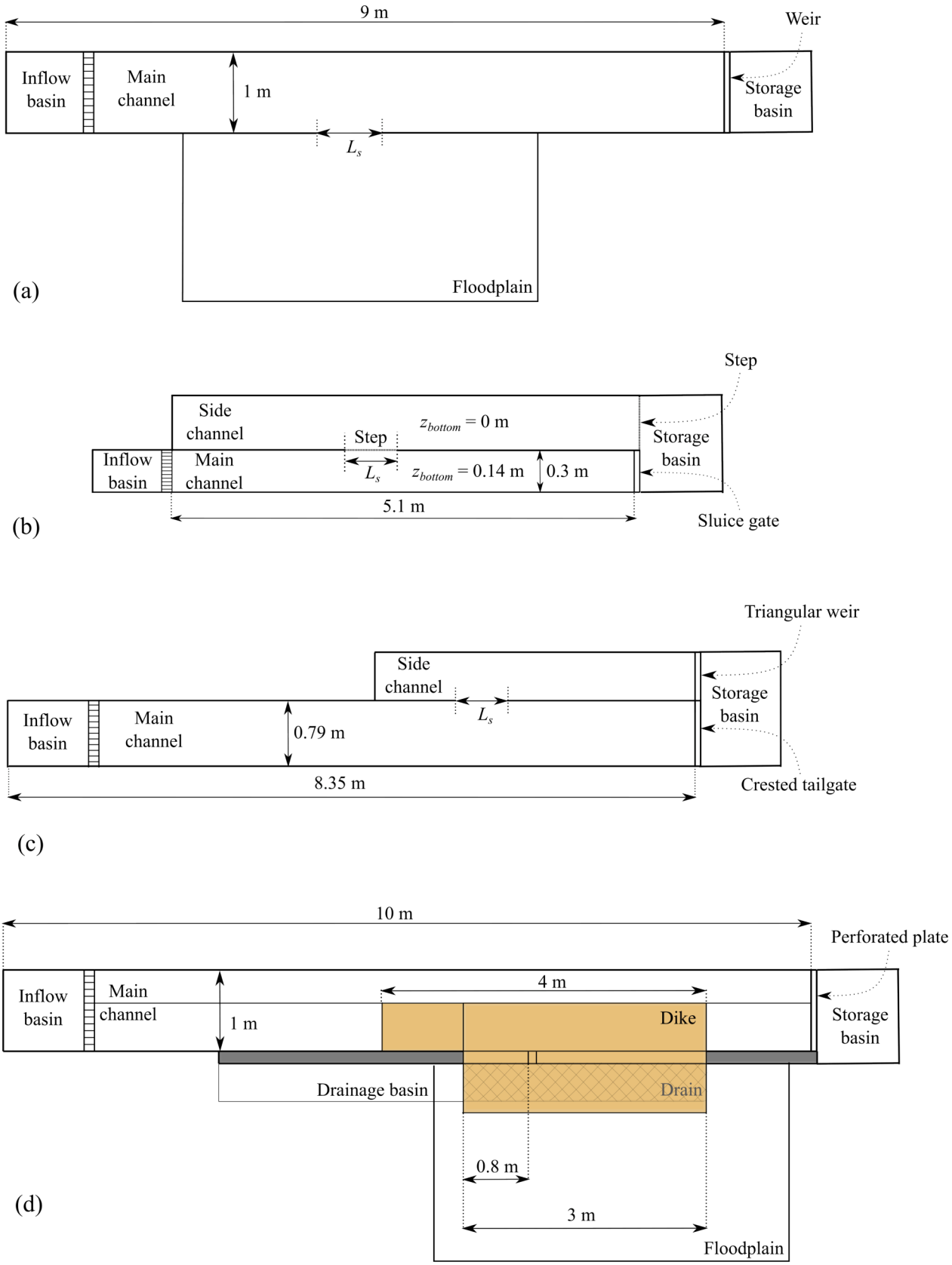

Fig. 3. Experimental setups used by (a) Roger et al. (2009), (b) Michelazzo et al. (2015), (c) Mignot et al. (2020), and (d) Rifai et al. (2017). The subfigures are adapted from the cited studies.

impermeable whitewash to ensure a uniform bed roughness over the entire setup. A small notch was carved at the crest of the dike to initiate erosion at this specific spot. Once the dike breach began forming, its evolution was monitored with a nonintrusive laser profilometry technique (Rifai et al., 2019). Rifai et al. (2017) conducted experiments for many inflow discharges and downstream boundary conditions. In this work, we focus on four experiments based on four different inflow discharges ranging from 0.02 m^3/s to 0.05 m^3/s. In all cases, a perforated plate was used at the flume downstream extremity to regulate the water level.

In the experiments of Rifai et al. (2017) the side opening evolved and grew bigger in time since the dike was made of sand that is eroded by the flow. In the cases with fixed geometry of the side opening, the lateral flow could be considered steady; however, in the experiments of Rifai et al. (2017) the flow that goes through the side opening depends on time. For each time step, the crest height of the side weir, i.e., the breach in the dike, was determined from a scanned longitudinal line in the middle of the dike in the transverse direction. The profile of the dike breach is typically irregular; however, the models require a single crest height, either for the whole dike breach for the lumped model or for each spatial step Δx for the spatially distributed model. For the spatially distributed model, the crest height of each spatial step was chosen equal to the breach elevation at the center of the step, which was obtained using a linear interpolation between scanning measurements of the breach (spatial resolution of 1 cm). The side weir equations were then applied on each one-dimensional cell individually. For the lumped model, a representative crest height was chosen equal to the 15th percentile of the elevation of the scanned points along the dike crest center line that were within the dike breach.

4. Results

Sections 4.1 and 4.2 present a comparison between the results obtained from the two numerical models of Section 1.1 coupled with the side weir discharge coefficients from Table 1 and the corresponding measurements from the experimental configurations with fixed and dynamic geometry of the side opening, respectively.

4.1. Side opening with fixed geometry

As shown in Fig. 4, for the four experimental cases of Roger et al. (2009), the lumped model performed better than the spatially distributed model in estimating the lateral discharge Q_b through the side opening for almost every C_d formula that was tested. A notable difference is that the spatially distributed model always underestimated Q_b, while the lumped model generated more variable results. This difference may be understood by considering that, in practice, the water level significantly drops in the vicinity of the side breach due to water acceleration. This trend is captured by the one-dimensional model. Conversely, the lumped model overestimates the water level close to the breach as it only considers an averaged value over the entire control volume. As a result, using Eq. (1) with the average water height in the lumped model leads to larger estimations of the breach discharge.

Both models, and particularly the spatially distributed model, performed better for the smaller discharge and the larger flow depth, i.e., for smaller inflow Froude number. The height of the side weir crest in the experiments of Roger et al. (2009) was zero and as a result the C_d formula of Bagheri et al. (2014) was not tested because the weir crest height, p, is used in the denominator. From the remaining discharge coefficient equations in Table 1, the equations of Subramanya and Awasthy (1972) and Borghei et al. (1999) with the lumped model performed best on average, while the spatially distributed model was most successful when coupled with the equation of Nadesamoorthy and Thomson (1972), followed by Yu-Tek (1972). The equation of Singh et al. (1994) performed worst with both models. However, it needs to be noted that while the discharge coefficient equations were compared

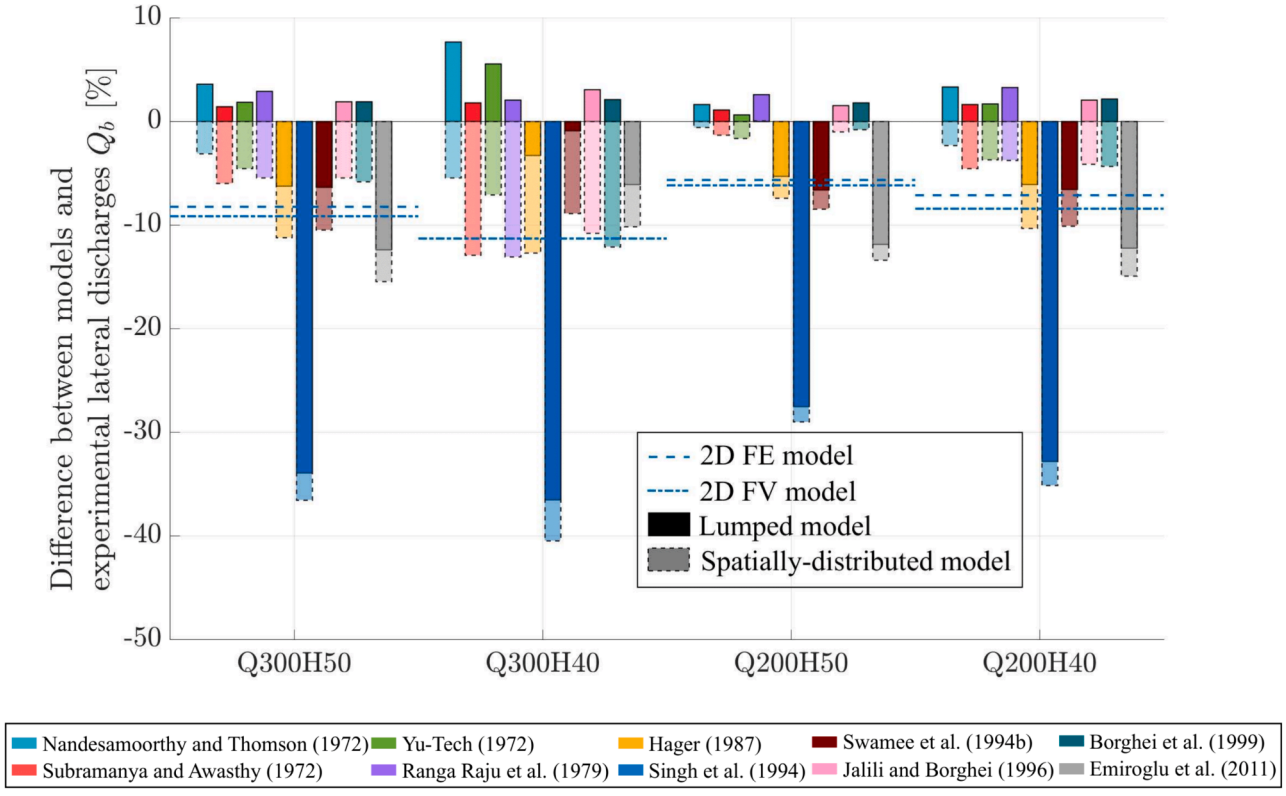

Fig. 4. Comparison between modelled and measured dike breach discharges, Q_b, for the experiments of Roger et al. (2009). The results from the 2D finite element (FE) and 2D finite volume (FV) models used by Roger et al. (2009) are also included in the comparison.

with the same data, the semi-empirical equations, such as the equation of Singh et al. (1994), were developed in different data ranges (Table 1). As a result, some of them were used out of their calibration range, which is the case with the Singh et al. (1994) formulation. Roger et al. (2009) also modelled their experiments with a 2D finite volume model and a 2D finite element model. The models underestimated the $\boldsymbol{Q_b}$ measurements by approximately 6 % to 12 % (Fig. 4). The absolute deviation of the 2D models from the measurements was larger than that of the lumped model, regardless of the $\boldsymbol{C_d}$ formula with the exception of Singh et al. (1994) and Emiroglu et al. (2011), and larger than most combinations of the spatially distributed model with a $\boldsymbol{C_d}$ formula (Fig. 4).

The experiments of Michelazzo et al. (2015) are similar to those of Roger et al. (2009) when considering the height of the side weir crest, which is also zero. However, in this case the length of the side weir is shorter as it varies from 3 cm to 47 cm. Contrary to the cases of Roger et al. (2009), in the experiments of Michelazzo et al. (2015) both the lumped model and the spatially distributed model mostly overpredicted the lateral discharge $\boldsymbol{Q_b}$, particularly as the length of the side weir increased (Fig. 5). The only consistent exception is the case where the models were coupled with the discharge coefficient equation of Singh et al. (1994), presumably because it was used outside of the data range for which it was developed. Overall, the accuracy of both models decreased as the side weir length increased. Another difference with the experiments of Roger et al. (2009) is that in the data of Michelazzo et al. (2015) the spatially distributed model performed better than the lumped model, for almost every coupled discharge coefficient equation. The discharge coefficient equation of Subramanya and Awasthy (1972) generated the best results when it was coupled with either of the two models. The rest of the discharge coefficient equations exhibited a rather erratic behavior when coupled either with the lumped model or the spatially distributed model. The formula of Bagheri et al. (2014) was again not tested because it is not applicable to a side weir with zero crest height.

With regard to the experiments of Mignot et al. (2020), for the cases with a fixed side opening with zero crest height there was considerable underestimation of the lateral discharge through the side opening on several occasions. The C_d equations that performed best were the same as those in the data of Roger et al. (2009), i.e., the equation of Subramanya and Awasthy (1972) for the lumped model and the equation of Nadesamoorthy and Thomson (1972) for the spatially distributed model. When the height of the crest of the side weir became non-zero, both models generated less accurate results compared to the zero crest height and underpredicted the experimental measurements by more than 25 % for most couplings with a discharge coefficient equation (Fig. 6). A notable exception was the coupling with the discharge coefficient equation of Singh et al. (1994), where both models performed much better. Overall, the lumped model performed better than the spatially distributed model for most cases of Mignot et al. (2020).

4.2. Side opening with dynamic evolution of its geometry

As shown in Fig. 7, for the four representative experimental cases of Rifai et al. (2017), the lumped model followed quite well the overall evolution trend of the discharge through the gradually augmenting dike breach, although in a less smooth way. The model did not capture accurately the discharge lowering after the initial peak in Test 1. For the lower upstream flow discharge, the discharge coefficient formulations did not have a significant impact on $\boldsymbol{Q_b}$; however, as the flow discharge increased the modelling results of $\boldsymbol{Q_b}$ exhibited a considerable scatter, particularly towards the end of each experiment when the dike breach was rather stabilized. Compared to the lumped model, the spatially distributed model predicted more accurately the initial peak of $\boldsymbol{Q_b}$ and was also able to reproduce the trend of the lateral discharge through the variable dike breach (Fig. 8). However, the modelled $\boldsymbol{Q_b}$ at the stabilization phase, after approximately 100 s, mostly underpredicted the measured values and gave worst results than the lumped model for the two lowest values of $\boldsymbol{Q_{in}}$, i.e., 20 and 30 l/s. The different discharge coefficient formulations that were tested in the spatially distributed model did not affect $\boldsymbol{Q_b}$ as much as they did in the lumped model, regardless of the upstream discharge that was prescribed in each experiment. The formulas of Emiroglu et al. (2011) and Bagheri et al. (2014) were not evaluated in this experiment because for the former there was no convergence in the numerical models and the latter is not applicable to a side weir with zero crest height.

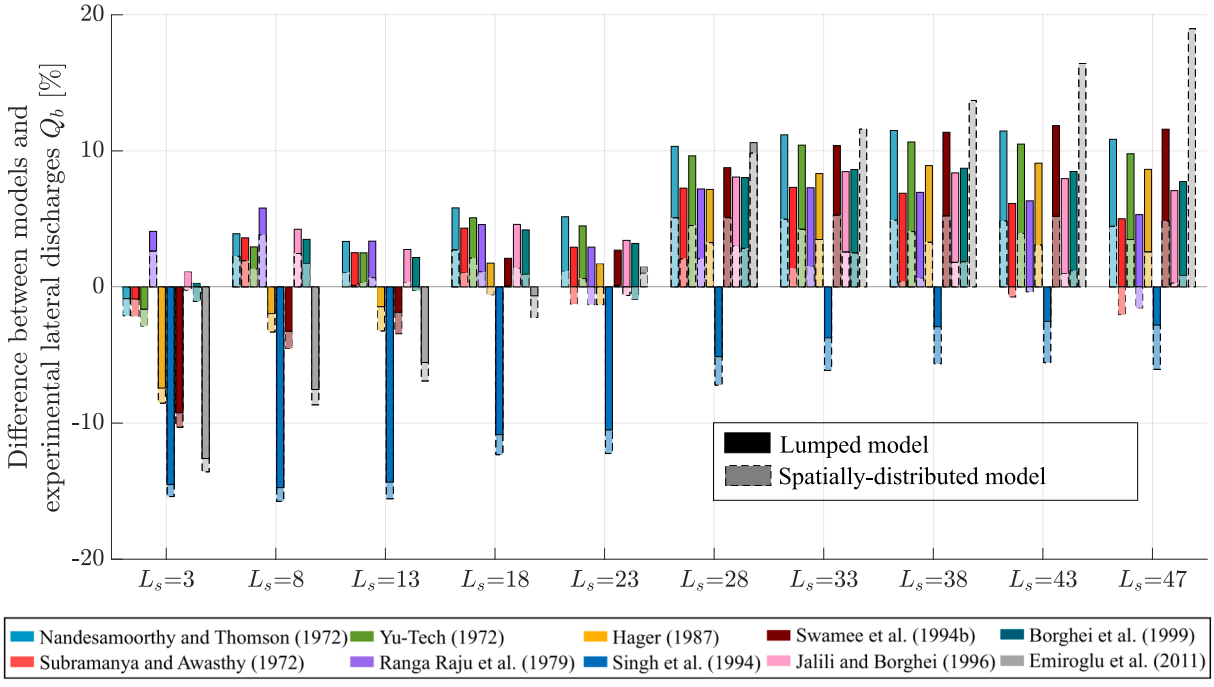

Fig. 5. Comparison between modelled and measured dike breach discharges, Q_b, for experiments of Michelazzo et al. (2015). The side opening widths, L_s, are in cm. No converged value could be obtained for $L_s \geq 33$ cm when using the formula of Emiroglu et al. (2011) in the lumped model.

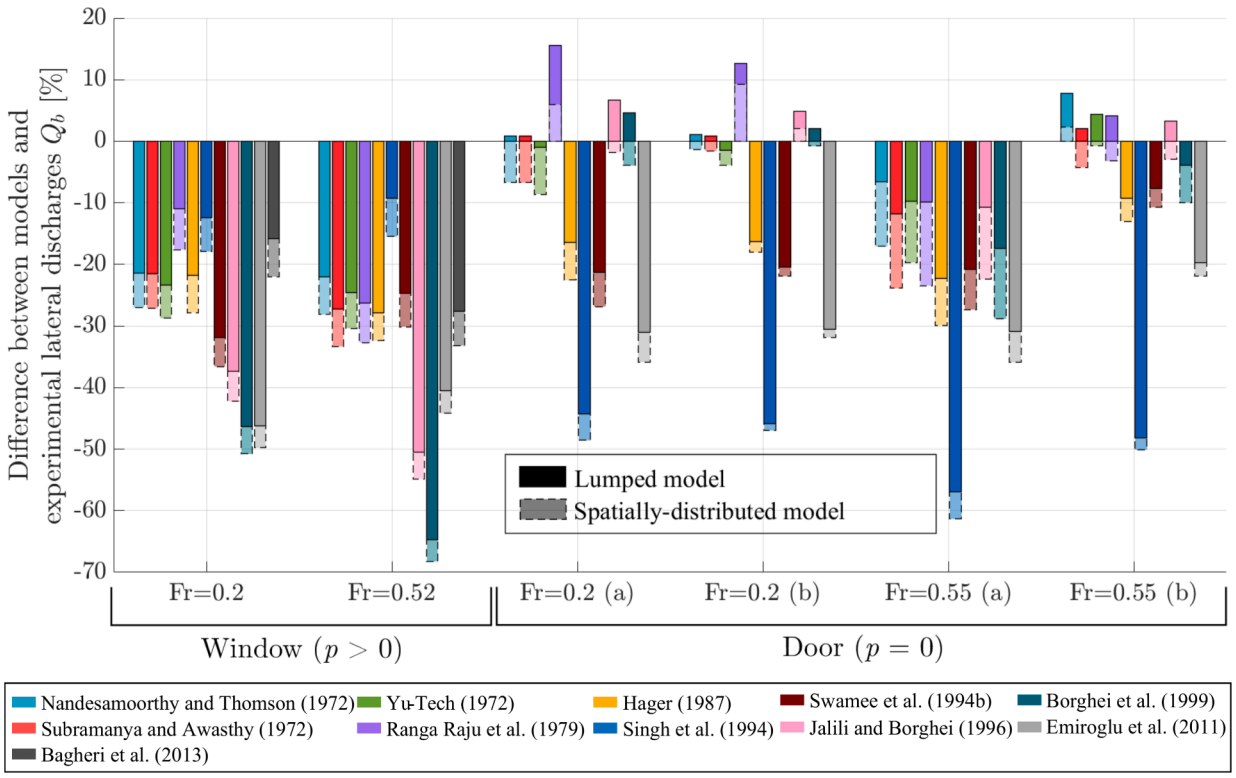

Fig. 6. Comparison between modelled and measured dike breach discharges, Q_b, for experiments of Mignot et al. (2020). Labels (a) and (b) refer to different combinations of inflow discharge and water height in the main channel but leading to the same Froude number.

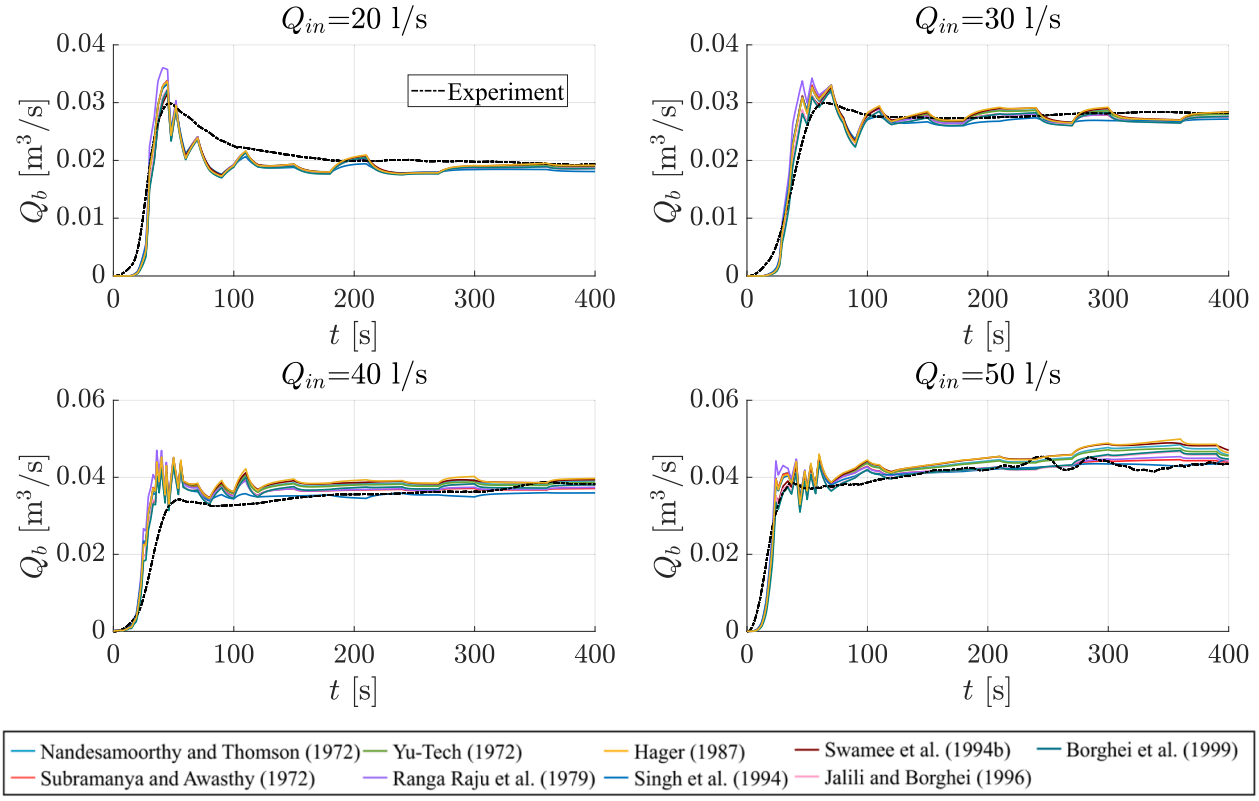

Fig. 7. Evolution of the dike breach discharge, Q_b, with the lumped model for experiments of Rifai et al. (2017). The formula of Emiroglu et al. (2011) did not converge and the formula of Bagheri et al. (2014) cannot be applied when $p = 0$.

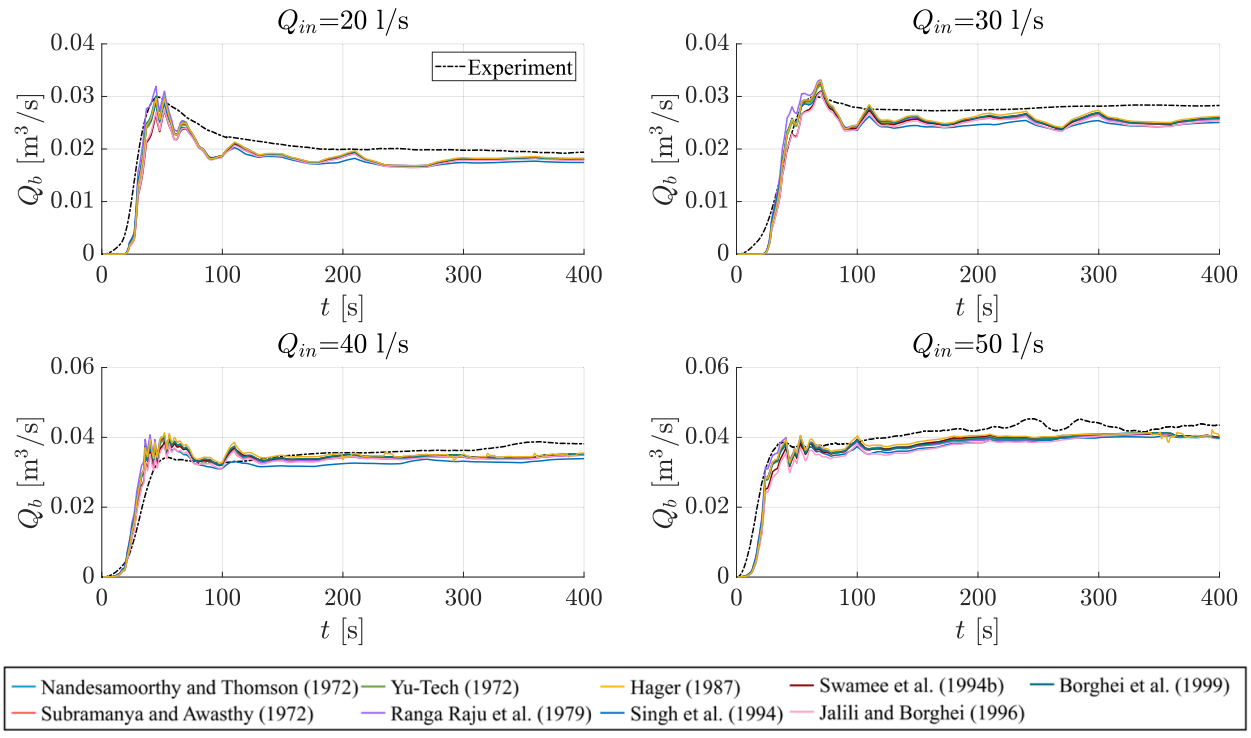

Fig. 8. Evolution of the dike breach discharge, Q_b, with the spatially distributed model for experiments of Rifai et al. (2017).

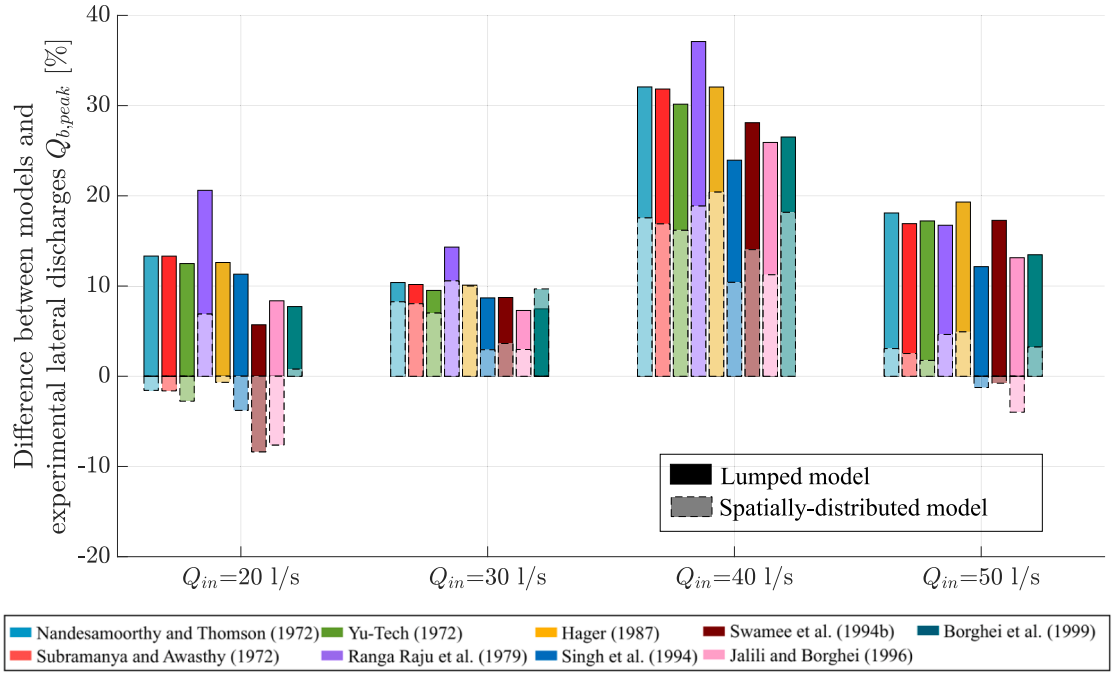

Fig. 9. Comparison between modelled and measured breach peak discharges, $Q_{b,peak}$, for experiments of Rifai et al. (2017).

The peak breach discharge, $Q_{b,peak}$, was more accurately predicted by the spatially distributed model (Fig. 9). Indeed, the lumped model led to an average absolute error that is more than two times higher than the absolute error of the spatially distributed model. The lumped model systematically overestimated the peak breach discharge, while the spatially distributed model sometimes underpredicted the peak lateral discharge. The discharge coefficient formulations that were tested exhibited a rather erratic behavior with respect to the different tests. Overall, the results of the different formulations exhibited greater variability compared to the previous cases with fixed openings and no formulation outperformed consistently the others when coupled with either of the two models.

5. Discussion

The estimation of the discharge coefficient in weir equations has typically a large empirical component that depends on the flow conditions of the laboratory experiments from which it was developed. As

such, weir equations can be confidently applied in data ranges for which they have been calibrated, but their performance outside these calibration ranges is uncertain. Fig. 10 shows how the range of the experimental data used in this study relate to the data ranges in which the semi-empirical equations for the estimation of C_d were developed. It is evident that in some cases, some formulations were used outside of their development range, which may be a reason for their deteriorating performance.

Ranga Raju et al. (1979) and Singh et al. (1994) used a 90° side channel as the side weir. The hinterland was thus confined as it corresponded to a relatively narrow perpendicular channel. In these cases, the predicted value of C_d should be underestimated compared to the case when the hinterland is not confined. This trend is very obvious for Singh et al. (1994) when considering a fixed breach geometry and a sharp crest. This formula performs better for Rifai et al. (2017), probably because there is a broad-crested weir in this case, which confines a bit the flow when it goes through the breach.

The implementation of the different models using the data of Roger et al. (2009) and Mignot et al. (2020) showed that increasing the model complexity, i.e., switch from a lumped to a discretized hydraulic description, does not always improve the accuracy of the side weir equation. This is the case not only when comparing our zero-dimensional lumped model to our one-dimensional model, but also when comparing to more detailed 2D models that Roger et al. (2009) used to simulate their experiments. A possible explanation for this result is that the flow near dike breaches has 3D features (Michelazzo et al., 2015) that can be more easily parameterized when modelled with a lower dimensionality model. Despite their simplicity, lumped models have exhibited a versatile and reliable behavior in a broad range of hydraulic applications, e.g., in interactions between surface flows and drainage systems (Kitsikoudis et al., 2021), and as such it is not surprising that such modelling tools perform relatively well when properly calibrated.

The importance of proper calibration of the discharge coefficient in lumped models becomes evident from the data from the experiments of Rifai et al. (2017), where the lumped model was outperformed by the spatially distributed model for the majority of discharge coefficient equations. The different discharge coefficient equations have been calibrated with data from laboratory experiments where the crest of the side weir was horizontal. In the experiments of Rifai et al. (2017) the dike breach, which was considered as a broad-crested side weir, exhibited an irregular cross-section at the different time-steps due to the spatial distribution of the erosion process induced by turbulent flow. In such cases with variability of the bed level across the dike breach, the

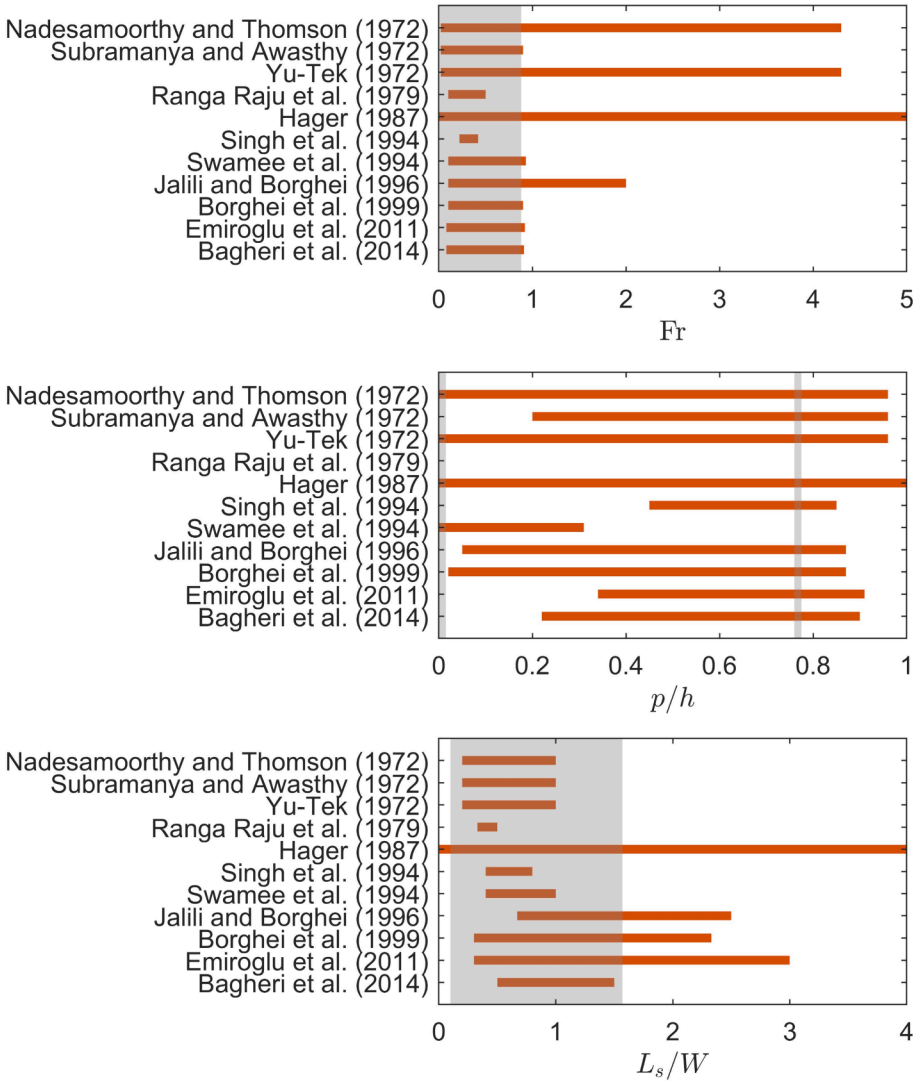

Fig. 10. Data ranges in which the semi-empirical discharge coefficient equations were developed. The grey shaded areas denote the ranges of the experimental data from the static side openings used in this study, i.e., the experiments of Rifai et al. (2017) are excluded. The formulation of Hager (1987) covers the whole range because it was developed based on theoretical arguments.

variations in flow depth will affect the discharge distribution over the dike breach (Michelazzo et al., 2018). In the experiments of Rifai et al. (2017), the lumped model was used by considering a straight weir crest at the 15th percentile of the elevation of the scanned points within the dike breach. This simplification led to a considerable overestimation of the breach peak discharge by the lumped model. This inaccuracy could also be attributed to sharp variations of the breach dimensions owed to sudden breach side slope failures, which instantaneously impact the value of C_d when using the empirical formulas. These sharp variations of C_d may also be the reason why the evolution of Q_b is smoother in the experiments compared to the modelling. The spatially distributed model predicted much better the peak discharge in the dynamic dike breach (Fig. 9), highlighting the importance of spatial discretization in cases with large spatial variability of the side opening.

For accurate hazard predictions related to fluvial dike breaching, a discretized model should be preferred. Nevertheless, the zero-dimensional model is more conservative as it tends to systematically overestimate the breach discharge (Fig. 7 and Fig. 9). To be on the safe side while optimizing the prediction accuracy, a trade-off consists in combining the one-dimensional model with a formulation that overestimates the breach discharge coefficient, e.g., the one proposed by Ranga Raju et al. (1979) or Borghei et al. (1999). It is also advised to test different formulations for the discharge coefficient to obtain an envelope curve, allowing for better uncertainty assessment.

6. Conclusions

Breaches in river dikes can pose a hazard of intense flooding to nearby areas. In such cases, flood risk assessment requires not only accurate modelling of the dike breach discharge towards the hinterland, but also fast modelling tools that can be used efficiently. To satisfy these requirements, in this study the flow through a breach in a dike with its axis parallel to a straight river reach was considered similar to the flow over a side weir. Eleven semi-empirical equations from the literature were tested for the parameterization of the discharge coefficient of the side weir equation, which was coupled to either a lumped model (zero-dimensional) or a spatially distributed model (one-dimensional). These models were tested in cases with increasing complexity: from cases with a fixed side opening with zero and non-zero crest height to a dynamic dike breach that evolves over time.

The performance of the different equations for the parametrization of the discharge coefficient of the side weir equation varied with the different cases, highlighting the empirical nature of most of them. The equations of Subramanya and Awasthy (1972) and Nadesamoorthy and Thomson (1972) performed best for a fixed opening with zero crest height while the equation of Singh et al. (1994) performed best for a fixed opening with non-zero crest height. For the cases with the dynamic dike breach, several formulations derived good results and there was no formula that was consistently superior. Overall, the modelling results were less accurate when transitioning from the fixed opening cases of zero to non-zero crest height and to the cases with a dynamic breach. Despite its simplicity, the lumped model generated better results than the spatially distributed model for many cases with fixed openings, but the spatially distributed model was more accurate in the dynamic breach cases. This highlights the importance of spatial discretization in cases where the dike breach exhibits irregular geometry. This model type should be selected when assessing hazard related to real-world dike breaching. For the sake of safety, it should be coupled with a formulation that overestimates the breach discharge coefficient, such as the one of Ranga Raju et al. (1979) or Borghei et al. (1999). Uncertainty may also be considered by creating an envelope curve for the breach discharge by testing different formulations for the breach discharge.

CRediT authorship contribution statement

Vincent Schmitz: Writing – review & editing, Visualization, Software, Methodology, Investigation, Formal analysis, Conceptualization. **Vasileios Kitsikoudis:** Writing – review & editing, Writing – original draft, Visualization, Formal analysis. **Gregoire Wylock:** Writing – original draft, Visualization, Software, Methodology, Investigation, Formal analysis, Data curation. **Sebastien Erpicum:** Software. **Michel Pirotton:** Methodology. **Pierre Archambeau:** Software. **Benjamin Dewals:** Writing – review & editing, Supervision, Methodology, Formal analysis, Conceptualization.

Declaration of competing interest

The authors declare that they have no known competing financial interests or personal relationships that could have appeared to influence the work reported in this paper.

Data availability

No data was used for the research described in the article.

References

Ahadiyan, J., Bahmanpouri, F., Adeli, A., Gualtieri, C., Khoshkonesh, A., 2022. Riprap Effect on Hydraulic Fracturing Process of Cohesive and Non-cohesive Protective Levees. Water Resour. Manag. 36, 625–639.

Al-Hafidh, I.A.I., Calamak, M., LaRocque, L.A., Chaudhry, M.H., Imran, J., 2022. Experimental Investigation of Flood Management by an Instantaneous Levee Breach. J. Hydraul. Eng. 148, 04021056.

ASCE/EWRI Task Committee on Dam/Levee Breaching, 2011. Earthen Embankment Breaching. J. Hydraul. Eng. 137, 1549–1564.

Bagheri, S., Kabiri-Samani, A.R., Heidarpour, M., 2014. Discharge coefficient of rectangular sharp-crested side weirs, Part I: Traditional weir equation. Flow Meas. Instrum. 35, 109–115.

Bomers, A., Schielen, R.M.J., Hulscher, S.J.M.H., 2019. Consequences of dike breaches and dike overflow in a bifurcating river system. Nat. Hazards 97, 309–334.

Borghei, S.M., Jalili, M.R., Ghodsian, M., 1999. Discharge Coefficient for Sharp-Crested Side Weir in Subcritical Flow. J. Hydraul. Eng. 125, 1051–1056.

D'Oria, M., Maranzoni, A., Mazzoleni, M., 2019. Probabilistic Assessment of Flood Hazard due to Levee Breaches Using Fragility Functions. Water Resour. Res. 55, 8740–8764.

Dazzi, S., Vacondio, R., Mignosa, P., 2019. Integration of a Levee Breach Erosion Model in a GPU-Accelerated 2D Shallow Water Equations Code. Water Resour. Res. 55, 682–702.

Dewals, B., Kitsikoudis, V., Mejía-Morales, M.A., Archambeau, P., Mignot, E., Proust, S., Erpicum, S., Pirotton, M., Paquier, A., 2023. Can the 2D shallow water equations model flow intrusion into buildings during urban floods? J. Hydrol. 619, 129231.

Echeverribar, I., Morales-Hernández, M., Brufau, P., García-Navarro, P., 2019. Use of internal boundary conditions for levees representation: application to river flood management. Environ. Fluid Mech. 19, 1253–1271.

Elalfy, E., Tabrizi, A.A., Chaudhry, M.H., 2018. Numerical and Experimental Modeling of Levee Breach Including Slumping Failure of Breach Sides. J. Hydraul. Eng. 144, 04017066.

Emiroglu, M.E., Agaccioglu, H., Kaya, N., 2011. Discharging capacity of rectangular side weirs in straight open channels. Flow Meas. Instrum. 22, 319–330.

Ferrari, A., Dazzi, S., Vacondio, R., Mignosa, P., 2020. Enhancing the resilience to flooding induced by levee breaches in lowland areas: a methodology based on numerical modelling. Nat. Hazards Earth Syst. Sci. 20, 59–72.

Haer, T., Husby, T.G., Botzen, W.J.W., Aerts, J.C.J.H., 2020. The safe development paradox: An agent-based model for flood risk under climate change in the European Union. Glob. Environ. Chang. 60, 102009.

Hager, W.H., 1987. Lateral Outflow Over Side Weirs. J. Hydraul. Eng. 113, 491–504.

Jalili, M.R., Borghei, S.M., 1996. Discussion: Discharge Coefficient of Rectangular Side Weirs. J. Irrig. Drain. Eng. 122, 132.

Kakinuma, T., Shimizu, Y., 2014. Large-Scale Experiment and Numerical Modeling of a Riverine Levee Breach. J. Hydraul. Eng. 140, 04014039.

Kamrath, P., Disse, M., Hammer, M., Köngeter, J., 2006. Assessment of Discharge through a Dike Breach and Simulation of Flood Wave Propagation. Nat. Hazards 38, 63–78.

Kerger, F., Archambeau, P., Erpicum, S., Dewals, B.J., Pirotton, M., 2011. A fast universal solver for 1D continuous and discontinuous steady flows in rivers and pipes. Int. J. Numer. Meth. Fluids 66, 38–48.

Kitsikoudis, V., Becker, B.P.J., Huismans, Y., Archambeau, P., Erpicum, S., Pirotton, M., Dewals, B., 2020. Discrepancies in Flood Modelling Approaches in Transboundary River Systems: Legacy of the Past or Well-grounded Choices? Water Resour. Manag. 34, 3465–3478.

Kitsikoudis, V., Erpicum, S., Rubinato, M., Shucksmith, J.D., Archambeau, P., Pirotton, M., Dewals, B., 2021. Exchange between drainage systems and surface flows during urban flooding: Quasi-steady and dynamic modelling in unsteady flow conditions. J. Hydrol. 602, 126628.

Li, X., Kitsikoudis, V., Mignot, E., Archambeau, P., Pirotton, M., Dewals, B., Erpicum, S., 2021. Experimental and Numerical Study of the Effect of Model Geometric Distortion on Laboratory Modeling of Urban Flooding. Water Resour. Res. 57 e2021WR029666.
Madsen, H., Lawrence, D., Lang, M., Martinkova, M., Kjeldsen, T.R., 2014. Review of trend analysis and climate change projections of extreme precipitation and floods in Europe. J. Hydrol. 519, 3634–3650.
Maranzoni, A., D'Oria, M., Mazzoleni, M., 2022. Probabilistic Flood Hazard Mapping Considering Multiple Levee Breaches. Water Resour. Res. 58 e2021WR030874.
Michelazzo, G., Oumeraci, H., Paris, E., 2015. Laboratory Study on 3D Flow Structures Induced by Zero-Height Side Weir and Implications for 1D Modeling. J. Hydraul. Eng. 141, 04015023.
Michelazzo, G., Oumeraci, H., Paris, E., 2018. New Hypothesis for the Final Equilibrium Stage of a River Levee Breach due to Overflow. Water Resour. Res. 54, 4277–4293.
Mignot, E., Camusson, L., Riviere, N., 2020. Measuring the flow intrusion towards building areas during urban floods: Impact of the obstacles located in the streets and on the facade. J. Hydrol. 583, 124607.
Nadesamoorthy, T., Thomson, A., 1972. Discussion of "Spatially Varied Flow over Side-Weirs. J. Hydraul. Div. 98, 2234–2235.
Onda, S., Hosoda, T., Jacimovic, N.M., Kimura, I., 2019. Numerical modelling of simultaneous overtopping and seepage flows with application to dike breaching. J. Hydraul. Res. 57, 13–25.
Orlandini, S., Moretti, G., Albertson, J.D., 2015. Evidence of an emerging levee failure mechanism causing disastrous floods in Italy. Water Resour. Res. 51, 7995–8011.
Ranga Raju, K.G., Gupta, S.K., Prasad, B., 1979. Side Weir in Rectangular Channel. J. Hydraul. Div. 105, 547–554.
Rifai, I., Erpicum, S., Archambeau, P., Violeau, D., Pirotton, M., El Kadi Abderrezzak, K., Dewals, B., 2017. Overtopping induced failure of noncohesive, homogeneous fluvial dikes. Water Resour. Res. 53, 3373–3386.
Rifai, I., El Kadi Abderrezzak, K., Erpicum, S., Archambeau, P., Violeau, D., Pirotton, M., Dewals, B., 2018. Floodplain Backwater Effect on Overtopping Induced Fluvial Dike Failure. Water Resour. Res. 54, 9060–9073.
Rifai, I., El Kadi Abderrezzak, K., Erpicum, S., Archambeau, P., Violeau, D., Pirotton, M., Dewals, B., 2019. Flow and detailed 3D morphodynamic data from laboratory experiments of fluvial dike breaching. Scientific Data 6.
Rifai, I., El Kadi Abderrezzak, K., Hager, W.H., Erpicum, S., Archambeau, P., Violeau, D., Pirotton, M., Dewals, B., 2021. Apparent cohesion effects on overtopping-induced fluvial dike breaching. J. Hydraul. Res. 59, 75–87.
Roger, S., Dewals, B.J., Erpicum, S., Schwanenberg, D., Schüttrumpf, H., Köngeter, J., Pirotton, M., 2009. Experimental and numerical investigations of dike-break induced flows. J. Hydraul. Res. 47, 349–359.
Schmitz, V., Erpicum, S., Abderrezzak, K. El kadi, Rifai, I., Archambeau, P., Pirotton, M., Dewals, B., 2021. Overtopping-Induced Failure of Non–Cohesive Homogeneous Fluvial Dikes: Effect of Dike Geometry on Breach Discharge and Widening. Water Resources Res. 57.
Schmitz, V., Arnst, M., El Kadi Abderrezzak, K., Pirotton, M., Erpicum, S., Archambeau, P., Dewals, B., 2023a. Global Sensitivity Analysis of a Dam Breaching Model: To Which Extent Is Parameter Sensitivity Case-Dependent? Water Resour. Res. 59 e2022WR033894.
Schmitz, V., Rifai, I., Kheloui, L., Erpicum, S., Archambeau, P., Violeau, D., Pirotton, M., El Kadi Abderrezzak, K., Dewals, B., 2023b. Main channel width effects on overtopping-induced non-cohesive fluvial dike breaching. J. Hydraul. Res. 61, 601–610.
Schmocker, L., Hager, W.H., 2012. Plane dike-breach due to overtopping: effects of sediment, dike height and discharge. J. Hydraul. Res. 50, 576–586.
Shustikova, I., Neal, J.C., Domeneghetti, A., Bates, P.D., Vorogushyn, S., Castellarin, A., 2020. Levee Breaching: A New Extension to the LISFLOOD-FP Model. Water 12, 942.
Singh, R., Manivannan, D., Satyanarayana, T., 1994. Discharge Coefficient of Rectangular Side Weirs. J. Irrig. Drain. Eng. 120, 814–819.
Stilmant, F., Pirotton, M., Archambeau, P., Roger, S., Erpicum, S., Dewals, B., 2013. Dike-break induced flows: a simplified model. Environ. Fluid Mech. 13, 89–100.
Subramanya, K., Awasthy, S.C., 1972. Spatially Varied Flow over Side-Weirs. J. Hydraul. Div. 98, 1–10.
Swamee, P.K., Pathak, S.K., Mohan, M., Agrawal, S.K., Ali, M.S., 1994. Subcritical Flow over Rectangular Side Weir. J. Irrig. Drain. Eng. 120, 212–217.
Tadesse, Y.B., Fröhle, P., 2020. Modelling of Flood Inundation due to Levee Breaches: Sensitivity of Flood Inundation against Breach Process Parameters. Water 12, 3566.
Tellman, B., Sullivan, J.A., Kuhn, C., Kettner, A.J., Doyle, C.S., Brakenridge, G.R., Erickson, T.A., Slayback, D.A., 2021. Satellite imaging reveals increased proportion of population exposed to floods. Nature 596, 80–86.
Viero, D.P., D'Alpaos, A., Carniello, L., Defina, A., 2013. Mathematical modeling of flooding due to river bank failure. Adv. Water Resour. 59, 82–94.
Vorogushyn, S., Merz, B., Apel, H., 2009. Development of dike fragility curves for piping and micro-instability breach mechanisms. Nat. Hazards Earth Syst. Sci. 9, 1383–1401.
Vorogushyn, S., Merz, B., Lindenschmidt, K.-E., Apel, H., 2010. A new methodology for flood hazard assessment considering dike breaches. Water Resour. Res. 46, W08541.
Wei, H., Yu, M., Wang, D., Li, Y., 2016. Overtopping breaching of river levees constructed with cohesive sediments. Nat. Hazards Earth Syst. Sci. 16, 1541–1551.
Wu, W., 2013. Simplified Physically Based Model of Earthen Embankment Breaching. J. Hydraul. Eng. 139, 837–851.
Wu, S., Yu, M., Wei, H., Liang, Y., Zeng, J., 2018. Non-symmetrical levee breaching processes in a channel bend due to overtopping. Int. J. Sedim. Res. 33, 208–215.
Yu, M., Wei, H., Liang, Y., Zhao, Y., 2013. Investigation of non-cohesive levee breach by overtopping flow. J. Hydrodyn. 25, 572–579.
Yu-Tek, L., 1972. Discussion of "Spatially Varied Flow over Side-Weirs. J. Hydraul. Div. 98, 2047–2048.